Available online at www.sciencedirect.com
ScienceDirect
Journal of Catalysis 251 (2007) 172–181
JOURNAL OF CATALYSIS
www.elsevier.com/locate/jcat

# Wet air oxidation of acetic acid over platinum catalysts supported on cerium-based materials: Influence of metal and oxide crystallite size

J. Mikulová, J. Barbier Jr. *, S. Rossignol, D. Mesnard, D. Duprez, C. Kappenstein

*University of Poitiers, LACCO UMR 6503, Laboratoire de Catalyse par les Métaux, 40 Avenue du Recteur Pineau, F-86022 Poitiers Cedex, France*

Received 12 March 2007; revised 5 June 2007; accepted 3 July 2007

Available online 30 August 2007

**Abstract**

Platinum catalysts (2.5 wt%) prepared by impregnation on pure commercial ceria and on $Zr_{0.1}(Ce_{0.75}Pr_{0.25})_{0.9}O_2$ sol–gel mixed oxide were synthesized and used for catalytic wet air oxidation (CWAO) of acetic acid. The influence of the platinum sintering (reducing treatment) was studied for both supports to modify the oxygen transfer from the gas phase onto the metallic active site of the catalyst and also to determine the effect of this treatment on the catalytic activity and stability. The catalysts were characterized by BET, TEM, XRD, FT-IR and hydrogen chemisorption before and after CWAO reaction, and oxygen storage capacity (OSC) was measured. The nature of the support [$CeO_2$ and $Zr_{0.1}(Ce_{0.75}Pr_{0.25})_{0.9}O_2$ compounds] and the preparation conditions led to samples displaying a Pt dispersion ranging from 0.4 to 41%, and BET surface area varying from 4 to 45 $m^2\,g^{-1}$. The results demonstrate poisoning of the catalysts during the CWAO experiments due to the formation of carbonate species. This limits the performance of the mixed oxide-based catalysts displaying the highest OSC values. A correlation was established between the OSC of the catalysts and the formation of carbonate species. Nevertheless, there is no correlation between OSC and catalytic activity, with the ceria-based samples showing the highest reaction rate. An optimal platinum crystallite size is required to achieve the highest conversion of acetic acid in terms of turnover frequency values.


*Keywords:* Platinum catalyst; CWAO; Ceria; XRD; FT-IR; Oxygen storage capacity

## 1. Introduction

Effective techniques for treating hazardous, toxic, and highly concentrated organic wastewaters are a necessity today, when water pollution is causing serious problems [1,2]. Several processes are currently available [3], including wet air oxidation (WAO), in which organic compounds are oxidized into carbon dioxide, water, and other innocuous end products. The WAO process has been adapted for wastewater with pollutant concentrations too low to be incinerated or too high to be treated biologically. This technique has not been widely used because of severe operating conditions and high costs [4]. WAO requires elevated pressures and temperatures, long residence times, and the use of materials that are resistant in highly corrosive conditions [2]. The use of catalysts can reduce the severity of WAO conditions [5,6]. Catalytic wet air oxidation (CWAO) also can improve pollutant conversion, lead to less critical corrosion problems, and decrease investment and operational costs. Heterogeneous catalysts are more desirable, because homogeneous catalysts require an additional separation step of soluble species (Cu or Fe compounds). The heterogeneous CWAO of organic pollutants has been reviewed by Levec and Pintar [7]. Transition metal oxides (including Cu, Fe, Co, Mn, Ni, Sn, and many other oxides in various combinations) and supported noble metals (including Pt, Pd, Ru, and Rh) have been proposed for the CWAO. For heterogeneous transition metal oxides, partial leaching of metal ions has been observed during the reaction, and a recovery step is necessary. Noble metal catalysts have proven their effectiveness for the CWAO of a wide range of pollutants, including carboxylic acids [3,8–10], phenol [11,12], and nitrogen compounds [13,14]. Different inert materials have been proposed as supports for CWAO catalysts, including various carbon-based supports [4,15,16] and metal oxide supports, such as $TiO_2$, $CeO_2$, and $ZrO_2$ [14,17–19]. Particular efforts have been

* Corresponding author. Fax: +33 (0) 5 49 45 37 41.
*E-mail address:* jacques.barbier.jr@univ-poitiers.fr (J. Barbier).

0021-9517/$ – see front matter 
doi:10.1016/j.jcat.2007.07.008

focused on studies involving CWAO by cerium-based heterogeneous catalysts [10,14,20–23]. Under conventional reaction conditions, oxygen is in deficient proportions (i.e., the limiting reactant) compared with the pollutants, and thus one of the essential steps in the reaction pathway corresponds to the oxygen mobility from the support to the active metal crystallites [9]. To improve the efficiency of the oxidation process, cerium-based heterogeneous catalysts have been widely studied, used, and developed due to their well-known oxygen storage capacity (OSC) and high oxygen mobility [21,24,25], especially in the case of gas-phase reactions [26,27].

Previous work in our laboratory [10], as well as other studies [28,29], have focused on the investigation of the role of cerium-based heterogeneous catalysts in the WAO of acetic acid. Using acetic acid as a model compound is justified by the fact that it is produced at the final stage of the WAO of various organic compounds. It is one of the most refractory compounds, and thus its oxidation is a rate-determining step for CWAO in many cases [7,30–32].

In this paper, we focus on platinum cerium-based catalysts and their activities in the WAO of acetic acid. Two types of platinum catalysts were prepared, one supported on ceria mixed with zirconium and praseodymium $Zr_{0.1}(Ce_{0.75}Pr_{0.25})_{0.9}O_2$ previously prepared in the laboratory [33] and the other supported on commercial pure ceria HSA 5 manufactured by Rhodia. The major drawback of the OSC performance of pure ceria is related to thermal resistance and low-temperature activity [34]. However, Zr cations can enhance the thermal stability of ceria without diminishing its high OSC [35,36]. Furthermore, Pr ions heavily modify the kinetics of oxygen transport, and thus permit more efficient redox processes at much lower temperatures [37]. In previous studies, we showed that the activities of Pt catalysts in CWAO are related to both OSC and deactivation by carbonate species, which are functions of metallic size, and thus an optimal platinum crystallite size is required [38].

The main objective of this research was to investigate the influence of metallic size of platinum supported on cerium-based materials on the CWAO of acetic acid by various characterizations before and after catalytic reaction tests. Both types of catalysts presented in this paper illustrate the range of metallic dispersions corresponding to different platinum metallic sizes.

## 2. Experimental

### 2.1. Catalyst preparation

All of the supports used, along with the abbreviations used, are presented in Table 1. $Zr_{0.1}(Ce_{0.75}Pr_{0.25})_{0.9}O_2$ was prepared by the sol–gel method, as described previously [33], using cerium(III) and praseodymium(III) nitrate and zirconium *n*-propoxide as precursors. Cerium oxide was a commercial rare earth ceria, HSA 5 (Rhodia). Both supports were calcined under static air for 5 h at 800 °C to stabilize the crystallite sizes before impregnation and reduction of the catalysts.

The impregnation and dry evaporation of 4.875 g of the support was carried out in a rotating evaporator with 12.5 mL of aqueous solution of $Pt(NH_3)_4(OH)_2$ (10 $g_{Pt}\,L^{-1}$) as a metal precursor salt, completed with distilled water to 39 mL (8 $mL_{H_2O}\,g^{-1}_{support}$). The concentration of the solution was calculated to obtain a metal content of 2.5 wt%. The samples were dried overnight at 120 °C and finally activated by reduction under $H_2$ (20 mL $min^{-1}$) for 3 h at 350, 500, 600, 650, 700, 800, and 900 °C to achieve different dispersions of Pt (Table 1).

Table 1
Abbreviations of supports and the 2.5 wt% platinum catalysts (number after support abbreviation shows the reduction temperature)

| Oxide support | Abbreviations | |
|---|---|---|
| | Supports | Pt catalysts reduced at different $T$ (°C) |
| $CeO_2$[a] | Ce | PtCe350, PtCe500, PtCe600, PtCe650, PtCe700, PtCe800, PtCe900 |
| $Zr_{0.1}(Ce_{0.75}Pr_{0.25})_{0.9}O_2$ | ZrCePr | PtZrCePr350, PtZrCePr500, PtZrCePr600, PtZrCePr650, PtZrCePr700, PtZrCePr800, PtZrCePr900 |

[a] Commercial Rhodia rare earth ceria HSA 5.

### 2.2. Catalyst testing

CWAO experiments were carried out in a 0.44-L Hastelloy C22 autoclave [39] equipped with a magnetic stirrer. The test batch contained 160 mL of aqueous solution of acetic acid (78 mmol $L^{-1}$) and 4 g $L^{-1}$ of catalyst; each experimental run took 3 h. The particle size in the catalyst powders was approximately 5 μm. To optimize the oxygen dissolution and permit good contact between the reactants and the catalytic powder dispersed in solution, the stirring rate of the turbine was 120 rpm. This stirring rate was chosen from the range of stirring rates corresponding to the kinetically limited regime to avoid the mass transfer-limited regime as well as overly violent stirring, which can cause mechanical damage to the catalyst and reactor [40]. To confirm that mass transfer was not the limiting factor, a specific study on a highly oxidative compound (oxalic acid) was performed in the same conditions as for acetic acid oxidation (COD 5 g $L^{-1}$) at an even lower temperature (140 °C). The results demonstrated total conversion to $CO_2$ in 15 min of reaction on the PtCe350 catalyst.

After an initial purge of the autoclave with helium, the autoclave was heated up to the reaction temperature of 200 °C. The reaction was initiated by adding 2 MPa of oxygen, which was kept constant during the whole experiment. Compared with the initial pollutant concentration (78 mmol $L^{-1}$) under these reaction conditions, oxygen in the solution was initially in a deficient proportion to limit metal overoxidation [16], but it was kept constant all along the run by the liquid/gas equilibrium (about 20 mmol $L^{-1}$) [40]. These reaction conditions are commonly used in CWAO. The progress of the reaction was followed by sampling and analyzing gas and liquid aliquots at appropriate intervals.

Gaseous samples were analyzed by a gas chromatograph equipped with a thermal conductivity detector. $CO_2$ was separated from other compounds on a Porapak Q packed column (0.6 mm i.d., 0.5 m long). Organic compounds of liquid samples were separated at 30 °C in $H_2SO_4$ (2 mmol $L^{-1}$) on an Aminex

HPX-87H organic acid analysis column (300 × 7.8 mm) and analyzed using a Thermofinnigan UV6000LP diode array UV–vis detector, coupled with a Thermofinnigan RI-150 refractive index detector [39]. The CWAO of acetic acid gave only $CO_2$ as a product.

From the results, the molar ratios of mineralization, activity, and turnover frequency (TOF) were calculated for each experiment. The mineralization molar ratio $M$ [Eq. (1)] corresponds to the ratio of the total $CO_2$ formed in CWAO ([$CO_2$] in mmol C $L^{-1}$) and the total initial amount of organic carbon ($TOC_i$ in mmol C):

$$M = \frac{[CO_2]}{TOC_i}. \tag{1}$$

$CO_2$ is formed according to

$$CH_3COOH + 2O_2 \rightarrow 2CO_2 + 2H_2O. \tag{2}$$

The catalytic activity ($A$) is the amount of $CO_2$ formed in 1 h of reaction per gram of metal (mmol $CO_2$ $g_{me}^{-1}$ $h^{-1}$),

$$A = \frac{100(M_{1\ h} - M_{\text{blank } 1\ h})[\text{acetic}]_i 2}{m_{\text{cata}} w_{\text{me}}}, \tag{3}$$

where $[\text{acetic}]_i$ is the initial concentration of pollutant (in mmol $L^{-1}$), 2 is the number of C atoms in $CH_3COOH$, $w_{\text{me}}$ is the wt% of metal, and $m_{\text{cata}}$ is the mass of catalyst per liter. The calculation of $A$ is obtained after deducting the mineralization value at 1 h for the blank experiment ($M_{\text{blank } 1\ h}$, on bare support).

TOF (in $h^{-1}$) is calculated from

$$\text{TOF} = \frac{A M_{\text{me}}}{10D}, \tag{4}$$

where $M_{\text{me}}$ is the molar weight of metal and $D$ is the metal dispersion (in %).

### 2.3. Characterization

The surface areas of the samples were determined from the nitrogen adsorption isotherms at −196 °C in an automated Micromeritics Tristar 3000 apparatus after evacuation for 2 h at 250 °C using a simple BET 7-point procedure at a $P/P_0$ ratio of 0.05–0.25. The complete adsorption and desorption isotherms have been obtained for few samples, leading to information about porous volume.

Diffractograms and crystallite sizes were determined by XRD experiments using a Siemens D 5005 powder $\theta$–$\theta$ diffractometer using Cu$K\alpha$ radiation ($\lambda_{K\alpha} = 0.154186$ nm) and a graphite backmonochromator. The XRD patterns were obtained under the following conditions: dwell time, 2 s; step, 0.04° or 0.02°; constant divergence slit, 1°. Crystalline phases were identified by comparison with Powder Diffraction File standards from ICDD. The average crystallite sizes ($d$) were calculated using Scherrer's equation,

$$d = \frac{K\lambda_{K\alpha}}{\beta_c \cos\theta}, \tag{5}$$

with $\beta_c = \sqrt{(\beta^2 - \beta_0^2)}$, where $\beta$ (in rd) is the half-maximum line breath of the analyzed material, $\beta_0$ (in rd) is the half-maximum line breath of a perfectly well-crystallized $LaB_6$ standard, $K = 0.9$, and $\theta$ is the Bragg angle for the diffraction peak considered. Only (111), (200), and (311) diffraction peaks were taken into account for the support phase. The most intense diffraction peak of platinum (111) displays an intensity that is too low to allow precise calculation of crystallite size; therefore, the average sizes of platinum crystallites were determined based on hydrogen chemisorption.

TEM measurements were carried out on Philips CM 120 microscope with a linear resolution of 3.5 Å. Metal dispersion of the catalysts was estimated by hydrogen chemisorption in a chromatographic microreactor at −85 °C. Hydrogen pulses (0.26 mL) were injected at regular intervals after reduction under $H_2$ (350 °C, 1 h) and degassing under argon (350 °C, 3 h) using ultra-pure $H_2$ and Ar (<1 ppm impurities) [41].

The crystallite sizes of platinum ($d$ in Å) were calculated using the cubic model [41] as follows:

$$d\ (\text{Å}) = \frac{5 \times 10^{26} M_{\text{Pt}}}{DNS_{\text{Pt}}\rho_{\text{Pt}}}, \tag{6}$$

where $M_{\text{Pt}}$ is the molar weight of metal (g $mol^{-1}$), $N$ is the Avogadro number ($6.023 \times 10^{23}$ $mol^{-1}$), $S_{\text{Pt}}$ is the atomic surface of metal (for platinum 8 $Å^2$), $\rho_{\text{Pt}}$ is the density of metal (for platinum 21.09 g $mL^{-1}$), and $D$ is the dispersion (in %).

OSC was measured at 400 °C under atmospheric pressure. The sample (5 mg) was continuously purged with helium (30 mL $min^{-1}$). Successive or alternate pulses (0.265 mL) of $O_2$ (Air Liquide, ⩽5 ppm total impurities) and CO (Air Liquide) were injected every 2 min [42]. The OSC was calculated from the CO consumption after the sample was stabilized in alternate pulses (CO/$O_2$) [36]. The number of oxygen atom layers [NL; Eq. (7)], involved in the process, was calculated on the basis of the theoretical number of accessible surface oxygen atoms [$OSC_{\text{surf}}$; Eq. (8)] and the OSC of metal [$OSC_{\text{me}}$; Eq. (9)]:

$$\text{NL} = \frac{\text{OSC}_{\text{meas}} - \text{OSC}_{\text{me}}}{\text{OSC}_{\text{surf}}}, \tag{7}$$

$$\text{OSC}_{\text{surf}} = \frac{bS}{Na^2}, \tag{8}$$

$$\text{OSC}_{\text{me}} = \frac{Dw_{\text{me}}}{M_{\text{me}} \times 10^4}. \tag{9}$$

In these equations, $S$ is the BET surface area ($m^2$ $g^{-1}$), $a$ is the lattice parameter of support [37], $N$ is the Avogadro number, and $b$ is the fraction of reducible elements (Ce + Pr) in the unit cell. $D$, $M_{\text{me}}$, and $w_{\text{me}}$ were defined previously [see Eqs. (3) and (4)]. This calculation is based on the following assumptions:

- All of the $Ce^{IV}$ or $Pr^{IV}$ atoms of the surface monolayer are reduced to oxidation state +III.
- The (100) faces are located at the surface [33] and contain 2 metal atoms and 4 oxygen atoms per unit surface area $a^2$ (a is cubic cell parameter, $a = 5.4138$ Å for Ce and

5.3913 Å for ZrCePr); therefore, one out of four oxygen atoms contributes to the OSC process, as indicated by

$$x\mathrm{CO(g)} + \mathrm{CeO_2(s)} \rightarrow \mathrm{CeO_{2-x}(s)} + x\mathrm{CO_2(g)} \quad (10)$$

and

$$\mathrm{CeO_{2-x}(s)} + \frac{1}{2}x\mathrm{O_2(g)} \rightarrow \mathrm{CeO_2(s)}. \quad (11)$$

- Oxygen atoms bonded to reducible elements are the only ones that contribute to the OSC.

FT-IR spectra were collected using a Perkin–Elmer spectrometer. The powder sample (10 mg) was dispersed in KBr (150 mg). Experimental conditions were as follows: acquisition time, 120 s; number of scans, 20; resolution, 4 $cm^{-1}$. To compare the carbonate loadings of each catalyst, the transmittance ($T$ in %) permits determination of the $CO_3^{2-}$ absorbance IR band per $m^2$ from Beer's equation,

$$\mathrm{Abs} = \frac{1}{S_{\mathrm{BET}}} \log \frac{100}{T}. \quad (12)$$

## 3. Results

### 3.1. Metal–support interaction

Table 2 gives the BET values of the supports after calcination at 800 °C, along with their crystallite sizes determined by XRD. Our experiments show that the specific surface area of initial HSA 5 ceria (190 $m^2\,g^{-1}$) decreased to 45 $m^2\,g^{-1}$ and the crystallite size increased from 6 nm to 13 nm due to sintering during calcination at 800 °C. The same effect was observed for the ZrCePr compound even though the crystallites of this support were more agglomerated (i.e., lower measured BET values than those obtained by calculation with a model of cubic crystallites). These results are in accordance with literature data [37,38,43]. Table 2 also presents platinum dispersion values and Pt crystallite sizes calculated for all of the catalysts. The BET surface areas and the support crystallite sizes calculated from XRD measurements display no significant differences before and after impregnation of platinum precursor and reduction in any samples, except those reduced at the highest temperatures (800 and 900 °C). The size of the support crystallites increased and consequently the BET values decreased (Table 2; Fig. 1). Nevertheless, Fig. 1 clearly demonstrates the positive effect of adding Zr and Pr ions on the thermal stability of the catalyst, where the decreases in specific area ratios for ZrCePr compounds are limited compared with those for pure ceria. A significant loss of surface area can be observed for PtZrCePr900, whereas in the case of pure ceria catalysts, it was already observed for PtCe800. At 900 °C, the BET value decreased to 5 $m^2\,g^{-1}$ for PtCe and 4 $m^2\,g^{-1}$ for PtZrCePr, most likely due to reduction and sintering of the support under $H_2$ at temperatures exceeding the support air-treatment temperature (800 °C).

Table 2
BET surface area, support crystallite size ($d_{sup}$), dispersion ($D$) and Pt crystallite size ($d_{Pt}$) for all samples

| Samples | BET ($m^2\,g^{-1}$) | $d_{sup}$[a] (nm) | $D$[b] (%) | $d_{Pt}$[c] (nm) |
|---|---|---|---|---|
| Ce | 45 | 13 | – | – |
| ZrCePr | 19 | 14 | – | – |
| PtCe350 | 45 | 13 | 41 | 2 |
| PtCe500 | 45 | 13 | 37 | 2 |
| PtCe600 | 43 | 13 | 27 | 4 |
| PtCe650 | 40 | 13 | 19 | 5 |
| PtCe700 | 35 | 15 | 11 | 9 |
| PtCe800 | 12 | 30 | 4 | 23 |
| PtCe900 | 5 | 38 | 0.4 | 230 |
| PtZrCePr350 | 18 | 14 | 20 | 5 |
| PtZrCePr500 | 17 | 14 | 18 | 5 |
| PtZrCePr600 | 17 | 15 | 13 | 7 |
| PtZrCePr650 | 16 | 16 | 11 | 9 |
| PtZrCePr700 | 14 | 14 | 9 | 10 |
| PtZrCePr800 | 12 | 22 | 5 | 20 |
| PtZrCePr900 | 4 | 28 | 0.5 | 190 |

[a] Determined by XRD measurements (estimated relative standard deviation: ±10%).
[b] $H_2$ chemisorption measurements [41] (estimated relative standard deviation: ±5%).
[c] Determined by $H_2$ chemisorption.

Dispersion data of platinum as a function of reduction temperature are presented in Fig. 2. Up to 650 °C, the catalysts supported on pure ceria displayed twice the dispersion and consequently smaller metallic size compared with the PtZrCePr samples; at higher temperatures, they displayed similar dispersion.

The TEM images (Fig. 3) are in agreement with the results of BET surface area measurements. Concerning the catalysts treated at 350 °C (Figs. 3a and 3c), the average crystallite sizes of the two supports were quite similar. After a reducing treatment at 800 °C, the ceria catalyst (Fig. 3b) was more sintered than the ZrCePr catalyst (Fig. 3d). The higher thermal stability of ZrCePr catalysts is evidenced in these images.

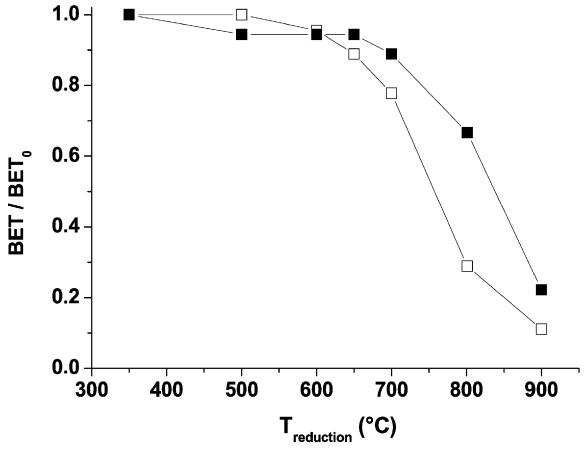


Fig. 1. Specific surface area ratio as a function of reduction temperature for the various 2.5 wt% platinum catalysts impregnated on (–□–) $CeO_2$ and (–■–) $Zr_{0.1}(Ce_{0.75}Pr_{0.25})_{0.9}O_2$ supports.

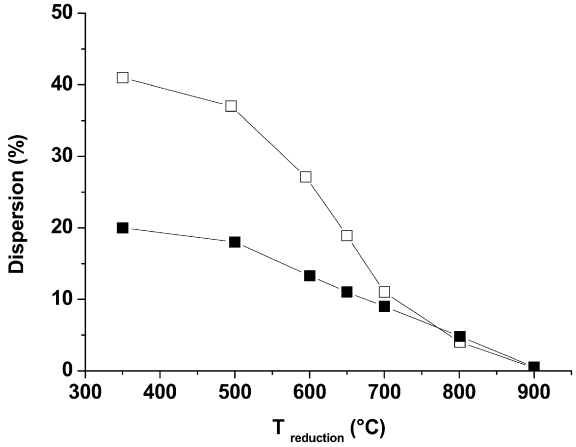


Fig. 2. Platinum dispersion as a function of reduction temperature for the various 2.5 wt% platinum catalysts impregnated on (–□–) $CeO_2$ and (–■–) $Zr_{0.1}(Ce_{0.75}Pr_{0.25})_{0.9}O_2$ supports.

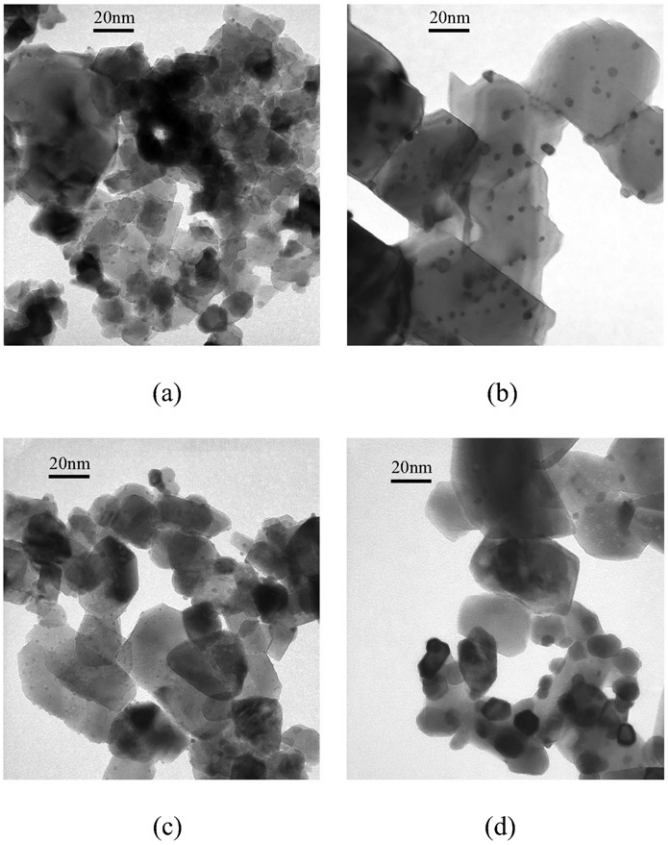


Fig. 3. TEM images of PtCe350 (a), PtCe800 (b), PtZrCePr350 (c) and PtZrCePr800 (d) catalysts.

### 3.2. Oxygen storage capacity

Fig. 4 illustrates $OSC/OSC_0$ values as a function of reduction temperature for 2.5 wt% platinum catalysts impregnated on $CeO_2$ and $Zr_{0.1}(Ce_{0.75}Pr_{0.25})_{0.9}O_2$ compounds; the $OSC_0$ values are OSC values of samples reduced at 350 °C. Table 3 shows OSC values and the calculated number of oxygen atoms layers involved in the OSC process (NL) for all samples. Previous studies have shown that thermal stability and OSC values are higher for ceria after the addition of zirconium and praseodymium cations [33]. The same phenomenon also can be observed for OSC values of PtCe (108 μmol $CO_2$ $g^{-1}$) and PtZrCePr (566 μmol $CO_2$ $g^{-1}$) catalysts after reduction at 350 °C. Compared with the bare supports, the impregnation of platinum on both supports enhanced the OSC [39]. The OSC values were stable up to 700 °C, but beyond this temperature, the sintering of the metallic phase and the support caused a decrease in these values. Nevertheless, the NL values show that whereas oxygen storage was limited to the first surface layer of pure ceria (NL near 1) even in the presence of the metal, the introduction of Zr and Pr cations greatly improved the redox process of the catalysts (6 > NL > 20), inducing the creation of anionic vacancies [37]. In this case, the bulk oxygen atoms were involved

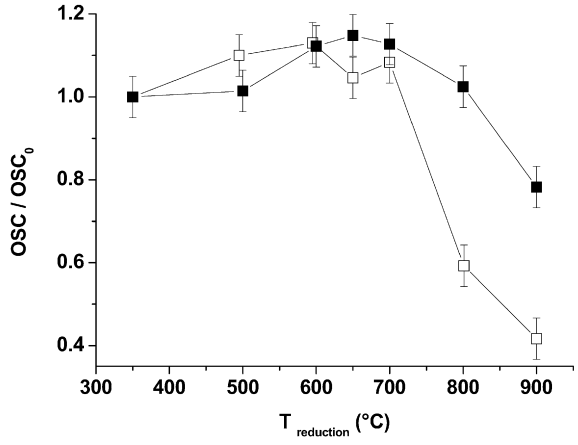


Fig. 4. $OSC/OSC_0$ values as a function of reduction temperature for the various 2.5 wt% platinum catalysts impregnated on (–□–) $CeO_2$ and (–■–) $Zr_{0.1}(Ce_{0.75}Pr_{0.25})_{0.9}O_2$ supports.

Table 3
OSC values and number of oxygen layers (NL) for all samples

| Samples | OSC (μmol $g^{-1}$) (accuracy (±5%)) | | | | NL |
|---|---|---|---|---|---|
| | Measured[a] | Metal[b] | Support[c] | Surface[d] | |
| Ce | 45 | 0 | 45 | 261 | 0.18 |
| ZrCePr | 176 | 0 | 176 | 97 | 1.82 |
| PtCe350 | 161 | 53 | 108 | 255 | 0.43 |
| PtCe500 | 161 | 47 | 114 | 255 | 0.45 |
| PtCe600 | 153 | 35 | 118 | 244 | 0.48 |
| PtCe650 | 137 | 24 | 113 | 227 | 0.50 |
| PtCe700 | 131 | 14 | 117 | 198 | 0.59 |
| PtCe800 | 69 | 5 | 64 | 68 | 0.94 |
| PtCe900 | 46 | 1 | 45 | 28 | 1.60 |
| PtZrCePr350 | 592 | 26 | 566 | 92 | 6.15 |
| PtZrCePr500 | 600 | 26 | 574 | 87 | 6.57 |
| PtZrCePr600 | 652 | 17 | 635 | 87 | 7.26 |
| PtZrCePr650 | 664 | 14 | 650 | 82 | 7.90 |
| PtZrCePr700 | 650 | 12 | 638 | 71 | 8.98 |
| PtZrCePr800 | 586 | 6 | 580 | 61 | 9.50 |
| PtZrCePr900 | 443 | 1 | 442 | 20 | 22.1 |

[a] OSC measured at 400 °C.
[b] Number of O atoms necessary for a complete oxidation of accessible Pt atoms (PtO).
[c] $OSC_{sup} = OSC_{meas} - OSC_{me}$.
[d] Theoretical number of reducible surface oxygen atoms.

in $O_2$ transfer as well. Below 800 °C, the reducing treatment did not change the NL values significantly. It seems that on these supports, the OSC was not significantly affected by the platinum and support crystallite size. A particularly interesting point is the ability of highly sintered PtZrCePr catalyst (reduction by $H_2$ at 900 °C) to transfer oxygen from the bulk to the surface even in the presence of very large crystallites of Pt ($D = 0.5\%$). At 900 °C, in contrast to the PtCe catalyst, for which the NL value is limited to 1 (total surface reduction), the NL of the PtZrCePr catalyst could reach much higher values. For ZrCePr supports, the contributions of Pr ions at both oxidation states ($Pr^{III}$ and $Pr^{IV}$) modified the kinetics of oxygen transfer, allowing a more efficient redox process.

### 3.3. Catalytic testing

Fig. 5 presents the results of catalytic testing for the PtCe350, PtCe900, PtZrCePr350, and PtZrCePr900 catalysts, in the form of mineralization percentage as a function time. The curve for the PtCe350 catalysts shows a higher mineralization rate than that for PtZrCePr350. Both catalysts reduced at 900 °C show very low mineralization rates, close to those obtained for the blank experiment (performed on bare supports). For the active catalysts (with reduction at 350 °C), the mineralization curves begin to flatten after 1 h of reaction, reflecting catalyst deactivation. To clarify the influence of the support and the reduction temperature, Fig. 6 presents the mineralization values (after 3 h of reaction time) versus the reduction temperature for all of the samples. As shown, the efficiency of platinum catalysts supported on well-dispersed ceria was enhanced until the reduction temperature reached 600 °C. As noted previously, platinum crystallites sintered as the reduction temperature increased, and thus the dispersion decreased. Beyond 600 °C, the effect of sintering became predominant, and larger platinum crystallites led to a decrease in the mineralization rate. On the other hand, catalysts supported on the ZrCePr compound display a lower mineralization activity, which decreased with increasing reduction temperature. Therefore, no direct correlation can be observed between OSC values and catalytic activity in the WAO of acetic acid.

Fig. 7 illustrates TOF values as a function of dispersion for the various platinum catalysts, showing optimum dispersion values for the PtCe (PtCe700) and PtZrCePr (PtZrCePr600) catalysts. The data corresponding to the 5% $Pt/Zr_{0.1}(Ce_{0.75}Pr_{0.25})_{0.9}O_2$ sample (support calcined at 500 °C and catalyst reduced at 350 °C) [39] supplement the curve of the PtZrCePr catalysts, confirming that the highly dispersed catalysts exhibited lower TOFs.

### 3.4. Structural data after reaction testing

Fig. 8 shows X-ray patterns ($20° < 2\theta < 45°$) of various PtCe and PtZrCePr catalysts before (Figs. 8a and 8c) and after 3 h of CWAO reaction (Figs. 8b and 8d). After reaction, some catalyst samples showed weak diffraction lines assigned to the formation of large crystallites of $Ce(CO_3)(OH)$ and

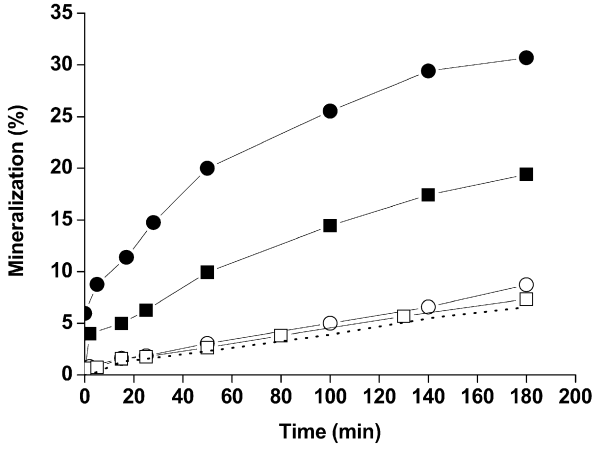


Fig. 5. Mineralization percentage as a function of time for (–●–) PtCe350, (–○–) PtCe900, (–■–) PtZrCePr350, (–□–) PtZrCePr900 catalysts and (···) ZrCePr or Ce supports.

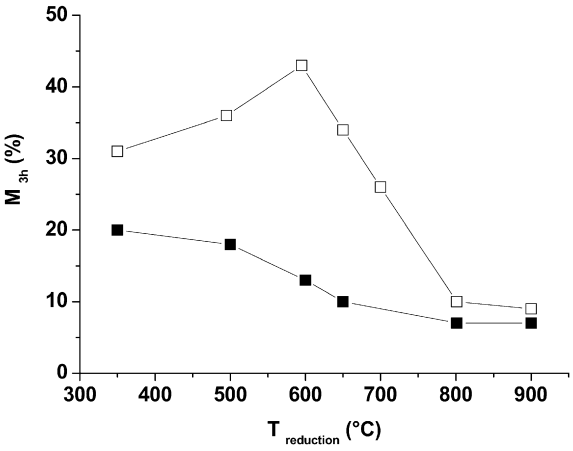


Fig. 6. Mineralization percentage after 3 h of reaction versus reduction temperature for the various platinum catalysts impregnated on (–□–) $CeO_2$ and (–■–) $Zr_{0.1}(Ce_{0.75}Pr_{0.25})_{0.9}O_2$ supports.

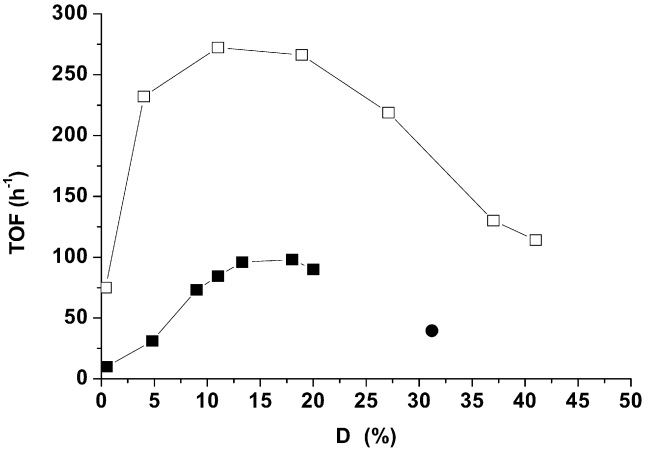


Fig. 7. TOF as a function of dispersion for the various platinum catalysts impregnated on (–□–) $CeO_2$, (–■–) $Zr_{0.1}(Ce_{0.75}Pr_{0.25})_{0.9}O_2$ supports and (●) $5\%Pt/Zr_{0.1}(Ce_{0.75}Pr_{0.25})_{0.9}O_2$ (support calcined at 500 °C and catalyst reduced at 350 °C).

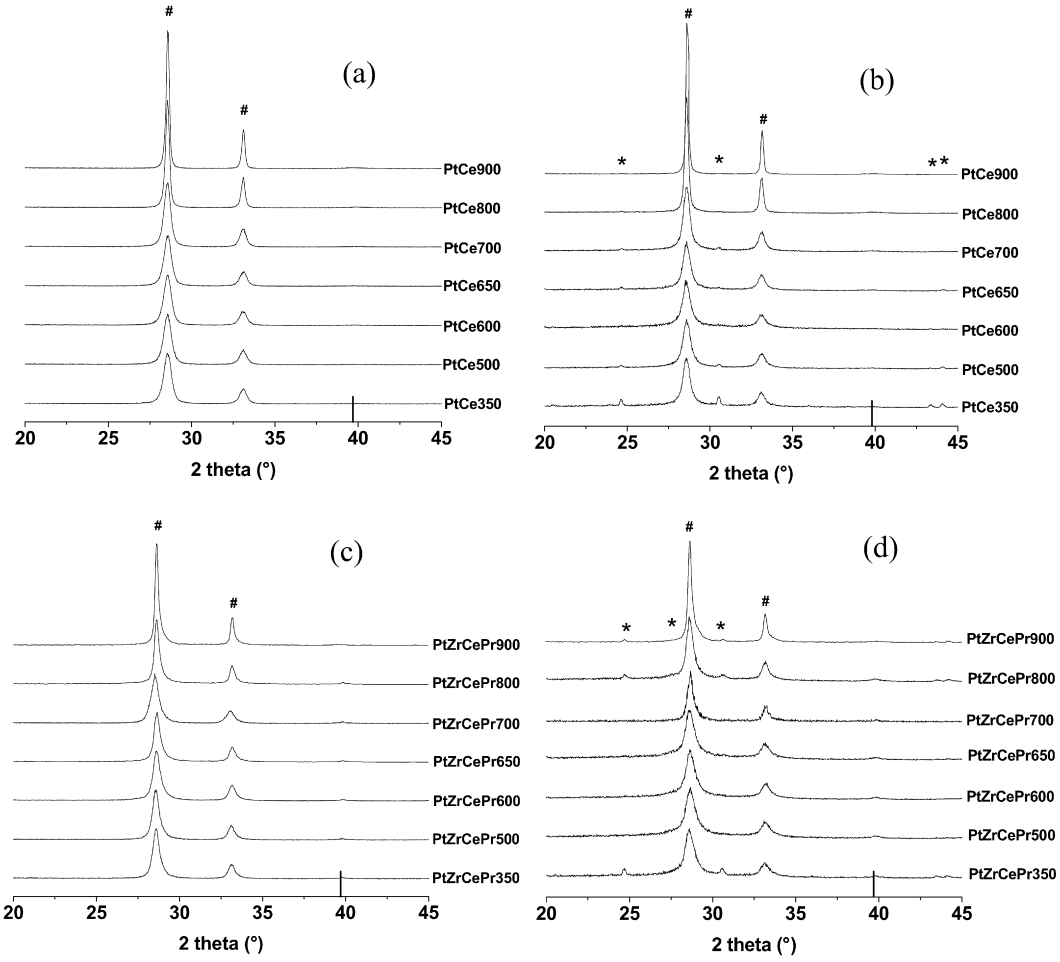


Fig. 8. X-ray patterns of various PtCe and PtZrCePr catalysts before (a, c) and after CWAO reaction (b, d). (#) PDF: 34-0394 $CeO_2$; (*) PDF: 52-0352 $Ce(CO_3)(OH)$ and PDF: 27-1376 $Pr(CO_3)(OH)$; (–) PDF: 04-0802 Pt.

$Pr(CO_3)(OH)$ (for samples containing Pr cations). These crystallites were 40–50 nm in size. They were present on the most dispersed catalyst (where the metal–support interface is higher) and on the sintered ZrCePr catalysts (which had the higher NL values). These results are directly related to those obtained by NL calculation in OSC measurements and indicate that effectively, acetic acid present in excess in the reaction medium can react directly with ceria, as demonstrated by the activity of bare supports (Fig. 5), inducing the formation of carbonate species and reduction of cerium atoms:

$$CH_3COOH(aq) + 8CeO_2(s) \rightarrow 2Ce(CO_3)OH(s) + 3Ce_2O_3(s) + H_2O(l). \quad (13)$$

The same behavior can occur with Pr cations, which also can be reduced, leading to $Pr(CO_3)(OH)$ species. The formation of such hydroxycarbonate species could be an inhibitor of oxygen transfer, which strongly limits the catalytic activities. XRD patterns reveal that the crystallite sizes of support remained constant during the run. Concerning noble metal stability, no leaching was detected by additional ICP-MS analyses.

Fig. 9 illustrates the IR spectra of PtCe and PtZrCePr samples before (Figs. 9a and 9c) and after (Figs. 9b and 9d) the catalytic reaction. Fig. 9a, for PtCe samples, reveals two main bands corresponding to surface bidentate carbonates ($\nu_{CO}$ = 1600 and 1310 $cm^{-1}$). Monodentate carbonates ($\nu_{CO}$ = 1530 and 1350 $cm^{-1}$) as well as hydrogen carbonates ($\nu_{CO}$ = 1630 and 1400 $cm^{-1}$) also can be observed [44,45]. Compared with pure ceria, the positions of the bands shifted very slightly to higher frequency when cerium atoms were replaced by zirconium and praseodymium atoms (Fig. 9c). This shift, which is characteristic of material presenting numerous vacancies, was induced by the cations (Zr and Pr) present in these structures [37]. Moreover, the intensities of the bands differed, indicating that carbonate species were not in the same proportion for the two supports; the presence of monodentate carbonates was favored on the PtZrCePr catalysts. Before reaction, the oxides contained surface hydrogen carbonate and carbonate species, because of the ability of these materials to adsorb the carbon dioxide related to their basic features [16]. Despite the fact that the proportions of various carbonate species seem quite different for each material, their evolution with the reducing treatment was similar. The band intensities decreased with the BET area values. After reaction (Figs. 9b and 9d), the spectra were more similar, in relation to the formation of bulk hydroxyl-carbonate; the bands corresponding to bidentate carbonates disappeared, and new bands attributed to polydentate species ($\nu_{CO}$ = 1460, 1440, and 1410 $cm^{-1}$) appeared. Hydro-

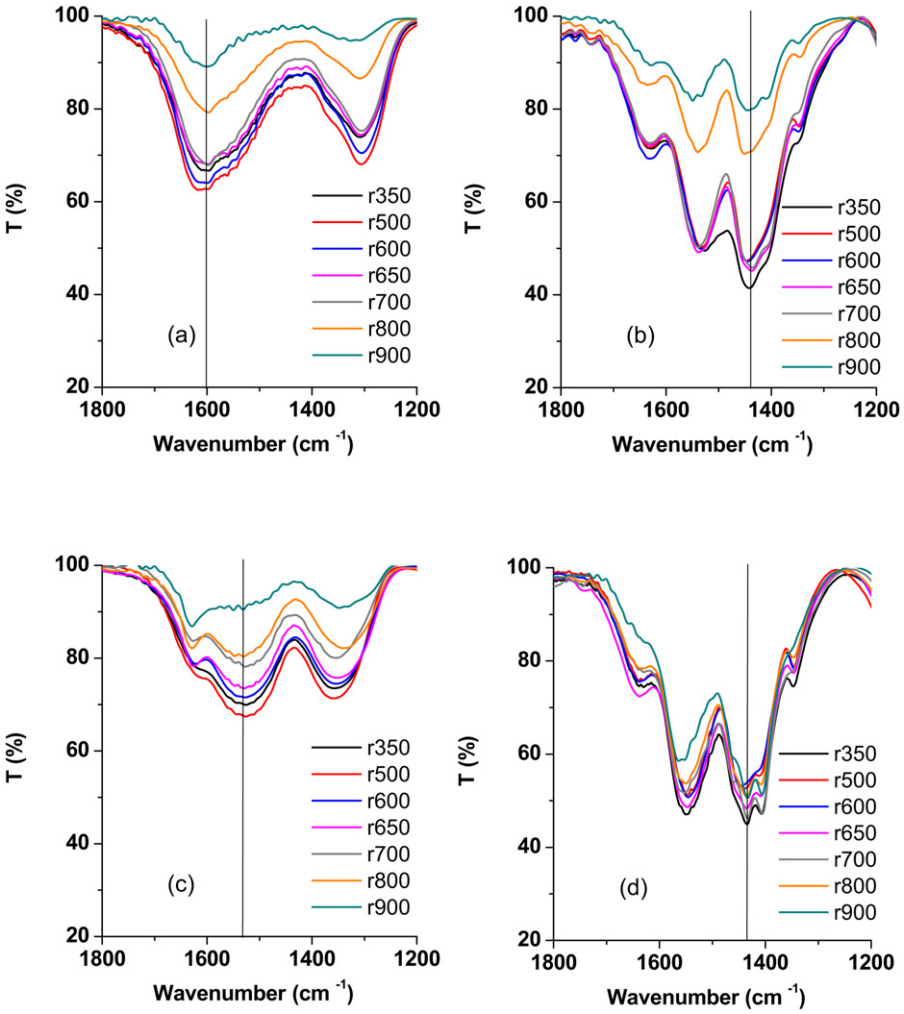


Fig. 9. Infrared spectra of PtCe (a, b) and PtZrCePr (c, d) catalysts before (a, c) and after (b, d) CWAO reaction. The vertical lines correspond to the wavenumbers used for the absorbance calculations.

gen carbonates and monodentate carbonates were present in both cases, in relation to the varying BET surface area of fresh catalysts. The carbonate band intensities were more pronounced on the PtZrCePr catalysts than on the PtCe catalysts reduced at 800 and 900 °C, confirming that higher OSC (Fig. 4) caused greater formation of carbonate species.

## 4. Discussion

The results obtained from the FT-IR technique depend on the specific surface area. To compare the amounts of carbonates, Fig. 10 presents maximal $CO_3^{2-}$ absorbances per $m^2$ (Abs). The calculations were performed from the values of FTIR transmittance indicated by the vertical lines in Fig. 9 for fresh PtZrCePr catalysts at 1530 $cm^{-1}$, fresh PtCe catalysts at 1600 $cm^{-1}$, and all used catalysts at 1440 $cm^{-1}$. This figure also displays the NL values of the various catalysts. For the fresh catalysts, the initial surface of carbonates per unit surface area level was low, regardless of the nature of the support. For the used catalysts, the amount of carbonates was strongly increased during the CWAO of acetic acid, particularly on ZrCePr compounds. It is important to note that the evolution of the amount of carbonate can be linked to the changes in NL values.

Both catalyst types reduced at 350 °C displayed high platinum dispersion values, which induced significant formation of carbonate species. The results obtained by the FT-IR and XRD confirm this finding. On the other hand, for the catalysts most affected by sintering (reduced at 900 °C), the behavior of the supports differed. For the $CeO_2$-supported catalyst, in which the OSC is limited to the surface, the level of carbonates per unit surface area was relatively low. For the ZrCePr catalyst, which displayed a very high NL value (>20), carbonate species formation affected both the surface and the bulk.

The catalysts reduced at intermediate temperatures (500–800 °C) showed a decrease in dispersion, limiting carbonate formation. FT-IR spectra and XRD patterns demonstrate the lower amount of these species. In this case, the structural characteristics were optimal to achieve high WAO efficiency.

Deactivation of the catalysts during CWAO was much more pronounced on the mixed-oxide support catalysts, regardless of the dispersions and BET surface areas. The XRD patterns (Fig. 8) clearly show the presence of $Ce(CO_3)(OH)$ or $Pr(CO_3)(OH)$ in the lattice. More importantly, the oxygen mi-

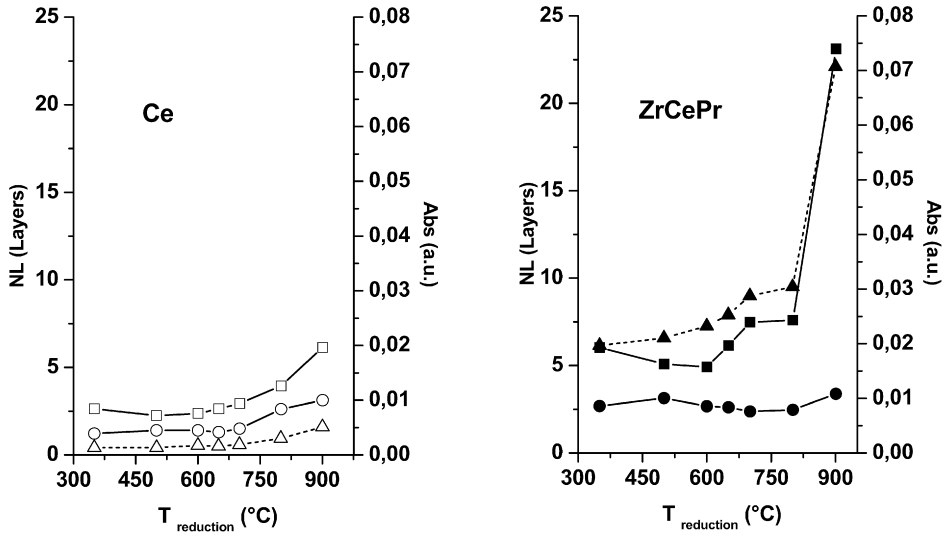


Fig. 10. $CO_3^{2-}$ absorbance IR band per $m^2$ [fresh Ce (–○–), fresh ZrCePr (–●–), used Ce (–□–), used ZrCePr (–■–) and NL values [Ce (···△···), ZrCePr (···▲···)] of catalysts.

gration capacity of the ZrCePr materials, as demonstrated by OSC measurements, was responsible for the drastic catalyst deactivation. The carbon dioxide formed during the WAO reaction was able to inhibit not only the surface, but also the heart of these materials through the formation of hydroxy-carbonate bulk species. Furthermore, optimal structural characteristics permit the minimization of $CO_2$ migration with maintenance of high oxygen transfer during the CWAO reaction. The result of this correlation is the bell-shaped curve of the evolution of TOF versus dispersion values for both supports. The optimum of the curve corresponds to the intermediately dispersed catalysts (obtained by the reducing treatment at 600–700 °C), which thus present the most favorable structures for the WAO of acetic acid.

## 5. Conclusion

One of the most limiting factors of the efficiency of catalytic WAO process is oxygen transfer from the gas phase to the noble metal active site, with migration of the oxygen species at the catalytic surface. To improve the oxidation process, two types of platinum catalysts were prepared by impregnation on pure commercial ceria and on mixed $Zr_{0.1}(Ce_{0.75}Pr_{0.25})_{0.9}O_2$ oxide. Zr cations are known to enhance the thermal stability of ceria without diminishing its high OSC values, and Pr ions are able to modify the kinetics of oxygen transport. The aim of this work was to study the sintering effect of $H_2$ treatment on catalyst performance. The Pt dispersion range of the catalysts was 41–0.5%, and the BET surface area varied from 45 to 4 $m^2\ g^{-1}$ according to the nature of the support. The catalysts were well characterized before and after catalytic WAO of the highly refractory acetic acid. Several characterization techniques (BET, TEM, XRD, FT-IR, OSC, and hydrogen chemisorption) were used to determine correlations between the catalyst structures and properties, as well as their performance in the CWAO of acetic acid. The main results of this study can be summarized as follows:

1. Zr and Pr ion doping had a beneficial effect on OSC as well as on the thermal stability of the catalysts.
2. A poisoning effect occurred during the catalytic testing. This effect, due to the formation of carbonates, limited the catalytic performance of the samples showing the highest OSC values in CWAO. Therefore, the PtZrCePr samples appeared less active than ceria-supported catalysts. For a given dispersion, the PtZrCePr catalysts had double the carbonate level as the PtCe samples.
3. A correlation was found between the OSC represented by NL calculations and the carbonate level.
4. An optimal platinum crystallite size was found to achieve the highest conversion of acetic acid in terms of TOF values. Consequently, no direct correlation between OSC values and catalytic WAO activity was seen for this type of catalyst.

## Acknowledgment

The authors thank Caroline Gendey for her help with catalyst preparation and testing.

## References

[1] K. Pirkanniemi, M. Sillanpää, Chemosphere 48 (2002) 1047.
[2] V.S. Mishra, V.V. Mahajani, J.B. Joshi, Ind. Eng. Chem. Res. 34 (1995) 2.
[3] F. Luck, Catal. Today 53 (1999) 81.
[4] D. Duprez, F. Delanoe, J. Barbier Jr., P. Isnard, G. Blanchard, Catal. Today 29 (1996) 317.
[5] S.T. Kolaczkowski, P. Plucinski, F.J. Beltran, F.J. Rivas, D.B. McLurgh, Chem. Eng. J. 73 (1999) 143.
[6] Y.I. Matatov-Meytal, M. Sheintuch, Ind. Eng. Chem. Res. 37 (1998) 309.
[7] J. Levec, A. Pintar, Catal. Today 24 (1995) 51.
[8] F. Luck, Catal. Today 27 (1996) 195.
[9] L. Oliviero, J. Barbier Jr., S. Labruquère, D. Duprez, Catal. Lett. 60 (1999) 15.
[10] J. Barbier Jr., F. Delanoë, F. Jabouille, D. Duprez, G. Blanchard, P. Isnard, J. Catal. 177 (1998) 378.
[11] A. Santos, P. Yustos, A. Quintanilla, S. Rodríguez, F. García-Ochoa, Appl. Catal. B 39 (2) (2002) 97.

[12] A. Cybulski, J. Trawczynski, Appl. Catal. B 47 (2004) 1.
[13] L. Oliviero, J. Barbier Jr., D. Duprez, Appl. Catal. B 1247 (2002) 1.
[14] J. Barbier Jr., L. Oliviero, B. Renard, D. Duprez, Catal. Today 75 (2002) 29.
[15] L. Oliviero, J. Barbier Jr., D. Duprez, A. Guerrero-Ruiz, B. Bachiller-Baeza, I. Rodriguez-Ramos, Appl. Catal. B 25 (2000) 267.
[16] Z.P.G. Masende, B.F.M. Kuster, K.J. Ptasinski, F.J.J.G. Janssen, J.H.Y. Katima, J.C. Schouten, Catal. Today 79 (2003) 357.
[17] C.B. Maugans, A. Akgerman, Water Res. 37 (2) (2003) 319.
[18] A. Pintar, M. Besson, P. Gallezot, Appl. Catal. B 30 (2001) 123.
[19] M. Besson, A. Kallel, P. Gallezot, R. Zanella, C. Louis, Catal. Commun. 4 (2003) 471–476.
[20] B. Renard, J. Barbier Jr., D. Duprez, S. Durécu, Appl. Catal. B 55 (2005) 1.
[21] S. Imamura, Ind. Eng. Chem. Res. 38 (1999) 1743.
[22] S. Imamura, Y. Okumura, T. Nishio, K. Utani, Ind. Eng. Chem. Prod. Res. Dev. 37 (1998) 1136.
[23] C. Milone, M. Fazio, A. Pistone, S. Galvagno, Appl. Catal. B 68 (1–2) (2006) 28.
[24] S. Imamura, Ind. Eng. Chem. Res. 38 (1999) 1743.
[25] A. Trovarelli, Catal. Rev. Sci. Eng. 38 (1996) 493.
[26] A. Trovarelli, C. de Leintenburg, M. Boaro, G. Dolcetti, Catal. Today 50 (1999) 359.
[27] A. Trovarelli, M. Boaro, E. Rocchini, C. de Leintenburg, G. Dolcetti, J. Alloys Compd. 323 (2001) 584.
[28] S. Hosokawa, H. Kanai, K. Utani, Y. Taniguchi, Y. Saito, S. Imamura, Appl. Catal. B 45 (2003) 181.
[29] S. Imamura, Y. Taniguchi, Y. Ikeda, S. Hosokawa, H. Kanai, H. Ando, React. Kinet. Catal. Lett. 76 (2002) 201.
[30] L. Oliviero, J. Barbier Jr., D. Duprez, H. Wahyu, J.W. Ponton, I.S. Matcalfe, D. Mantzavinos, Appl. Catal. B 35 (2001) 1.
[31] P. Gallezot, S. Chaumet, A. Perrard, P. Isnard, Catal. Today 168 (1997) 104.
[32] H. Delvin, I. Harris, Ind. Eng. Chem. Fund. 23 (1984) 387.
[33] S. Rossignol, C. Descorme, C. Kappenstein, D. Duprez, J. Mater. Chem. 11 (2001) 2587.
[34] S.J. Schmieg, D.N. Belton, Appl. Catal. B 6 (1995) 127.
[35] J. Kaspar, P. Fornasiero, M. Graziani, Catal. Today 50 (1999) 285.
[36] S. Rossignol, Y. Madier, D. Duprez, Catal. Today 50 (1999) 261.
[37] S. Rossignol, D. Mesnard, F. Gérard, C. Kappenstein, D. Duprez, J. Mater. Chem. 13 (2003) 3017.
[38] J. Mikulová, S. Rossignol, J. Barbier Jr., D. Duprez, C. Kappenstein, Catal. Today 124 (2007) 185.
[39] J. Mikulová, S. Rossignol, J. Barbier Jr., D. Mesnard, D. Duprez, C. Kappenstein, Appl. Catal. 72 (2007) 1–10.
[40] S.D. Cramer, Ind. Eng. Chem. Proc. Des. Dev. 19 (1980) 300.
[41] D. Duprez, J. Chim. Phys. 80 (1983) 487.
[42] S. Kacimi, J. Barbier Jr., R. Taha, D. Duprez, Catal. Lett. 22 (1993) 343.
[43] T. Kobayashi, S. Iwamoto, M. Inoue, J. Alloys Compd. 9 (2006) 1149.
[44] C. Binet, M. Daturi, J.C. Lavalley, Catal. Today 50 (1999) 207.
[45] O. Pozdnyakova, D. Teschner, A. Woostsch, J. Krohnert, B. Steinhauer, H. Dauer, L. Toh, F.C. Jentoft, A. Knop-Gericke, Z. Paal, R. Schlogl, J. Catal. 237 (2006) 1.